PHYSICAL REVIEW B **77**, 214407 (2008)

Exotic (anti)ferromagnetism in single crystals of $Pr_6Ni_2Si_3$

Y. Janssen,* K. W. Dennis, R. Prozorov, P. C. Canfield, and R. W. McCallum
Ames Laboratory DOE and Department of Physics and Astronomy, Iowa State University, Ames, Iowa 50011, USA
(Received 8 January 2008; revised manuscript received 6 May 2008; published 4 June 2008)

The ternary intermetallic compound, $Pr_6Ni_2Si_3$, is a member of a structure series of compounds based on a triangular structure where the number of Pr atoms in the prism cross section can be systematically varied. $Pr_6Ni_2Si_3$ contains two distinct Pr lattice sites which result in complex interactions between the magnetic ions. Extensive measurements of specific heat and magnetization on single-crystal samples indicate that $Pr_6Ni_2Si_3$ orders with both a ferromagnet and an antiferromagnet component, with ordering temperatures of 39.6 and ~32 K, respectively. The ferromagnetic component $\parallel c$ axis is accompanied by a large hysteresis, and the antiferromagnetic component $\perp c$ axis is accompanied by a spin-flop-type transition. More detailed measurements, of the vector magnetization, indicate that the ferromagnetic and the antiferromagnetic order appear independent of each other. These results not only clarify the behavior of $Pr_6Ni_2Si_3$ itself but also of the other members of the structure series, $Pr_5Ni_2Si_3$ and $Pr_{15}Ni_7Si_{10}$.

DOI: 10.1103/PhysRevB.77.214407 PACS number(s): 75.50.−y, 75.30.Gw, 75.10.−b

I. INTRODUCTION

A magnetic local-moment rare-earth system with rare-earth moments on nonequivalent crystallographic sites may be difficult to analyze experimentally. Different interatomic spacings may, through the oscillatory Ruderman–Kittel–Kasuya–Yosida (RKKY) interaction mechanism,[1] lead to magnetic interactions with different signs and strengths. Different site symmetries and local environments may lead to different crystalline-electric-field (CEF) splittings and therefore to different magnetic anisotropies, see, e.g., Ref. 2. In such systems, the RKKY interactions and the CEF splittings may create complex magnetic ordering. If, however, the considered magnetic system forms part of a series, similarities in magnetic properties of the members may lead to a greater understanding of the properties of all members. Rare-earth intermetallic compounds often form natural series because, due to the chemical similarity of rare earths, a particular rare earth can be replaced for another, and the resulting magnetic systematics can be appreciated (see, e.g., Ref. 3). Another type of series that may be considered is the structure series. In a structure series, structural features are systematically repeated, which may help in understanding the physical properties of members of such series.

In 1984, Parthé and Chabot[4] reviewed the crystal structures of ternary rare-earth (R) transition-metal (T) silicide and boride (M) compounds. At that time, about 80 different compositions were known. A number of the R-T-M compounds can be classified as part of a structure series. The majority of these structural series consist of layered structures, and the organization of the layers distinguishes members. However, there are also at least two R-T-M structure series where the basic building block is a triangular prism. These prisms may be assembled into larger prisms in a geometric progression where each member of this progression represents a unique crystal structure with a specific ratio of rare earth to transition-metal atoms. The two known series of this type are described by the formulas $R_{\frac{1}{2}n(n+1)}T_{3(n^2+1)}M_{2n^2+1}$, with as $n=2$ member UCo_5Si_3, and $R_{(n+2)(n+1)}Ni_{n(n-1)+2}Si_{n(n+1)}$, with as $n=2$ member the title compound $Pr_6Ni_2Si_3$ (Fig. 1). In the former series, there is only a single rare-earth site, so the potential for competing interactions is small. In addition, the low concentration of both rare-earth and transition-metal ions is expected to result in weak magnetic interactions and low ordering temperatures. On the contrary, the latter series consists of, besides some 20% nonmagnetic Ni, see below, roughly 50% rare earth and, moreover, R occupy different crystallographic sites and different local environments, see, e.g., Refs. 6–9.

The known members of the series of $Pr_{(n+2)(n+1)}Ni_{n(n-1)+2}Si_{n(n+1)}$ compounds are $Pr_6Ni_2Si_3$ ($n=2$), $Pr_5Ni_2Si_3$ ($n=3$), and $Pr_{15}Ni_7Si_{10}$ ($n=4$). Their structure is hexagonal, with space group $P63/m$, and the Pr ions occupy different independent crystallographic sites. For $Pr_6Ni_2Si_3$, the Pr ions occupy two independent low-symmetry 6h sites, denoted in Fig. 1 as Pr1 and Pr2 ("corner" and "edge" in Ref. 9). For $Pr_5Ni_2Si_3$, the Pr ions occupy three independent 6h sites and one 2d site, where two of the 6h sites are compa-

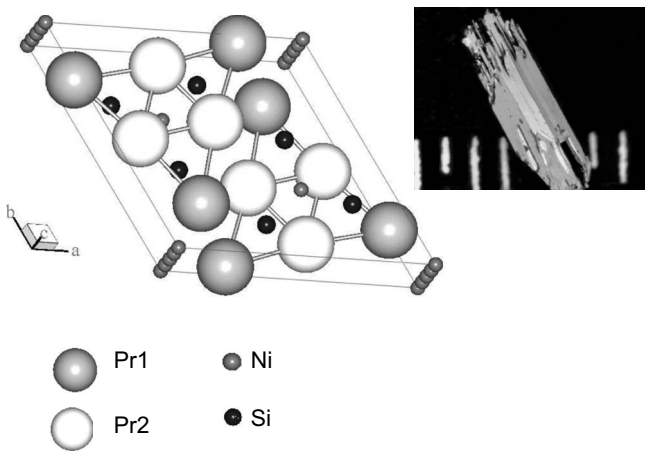

FIG. 1. Schematic drawing (Ref. 5) of the $Ce_6Ni_2Si_3$-type unit cell of $Pr_6Ni_2Si_3$. Note that the Ni sites on the edges of the unit cell are not fully occupied (Ref. 6). The inset shows a photograph of a self-flux-grown crystal of $Pr_6Ni_2Si_3$ on a background with a millimeter scale. The crystal axis is the c axis, and a [110] facet is facing the reader.

rable to the two 6*hs* in $Pr_6Ni_2Si_3$ (Pr1 and Pr2 in Fig. 1). For $Pr_{15}Ni_7Si_{10}$, Pr ions occupy five independent 6*h* sites. Two of these are comparable to the two 6*hs* of $Pr_6Ni_2Si_3$. More details on the stoichiometry and the complex crystal structures of the members of the structure series are discussed by Wu *et al.*[6]

Results from polycrystalline samples[7–11] indicate that all members of the structure series show ferromagnetic order, involving Pr magnetic moments only. The Curie temperature was found close to 40 K (Ref. 9) for $Pr_6Ni_2Si_3$, 50 K (Refs. 7–11) for $Pr_5Ni_2Si_3$, and 60 K (Refs. 8, 10, and 11) for $Pr_{15}Ni_7Si_{10}$. In polycrystalline $Pr_5Ni_2Si_3$ and $Pr_{15}Ni_7Si_{10}$, the development of a significant coercivity has been observed.[7,8] A second lower-temperature transition has been observed by both specific heat and magnetostriction in $Pr_5Ni_2Si_3$ and $Pr_{15}Ni_7Si_{10}$, at ~25 K and at ~33 K, respectively. These lower-temperature transitions have been interpreted as due to spin-reorientations.[8,10] From field-dependent specific heat on polycrystalline $Pr_5Ni_2Si_3$, it was concluded that the 25 K anomaly has an antiferromagnetic character. Magnetization loops of both $Pr_5Ni_2Si_3$ and $Pr_{15}Ni_7Si_{10}$, at temperatures below their respective lower-temperature transitions, show metamagneticlike anomalies, close to 3 T for $Pr_5Ni_2Si_3$ at 5 K, and close to 4 T for $Pr_{15}Ni_7Si_{10}$ at 5 K, which can also be interpreted as due to the presence of both ferromagnetic and antiferromagnetic characters in the magnetic order.[7] These anomalies are more pronounced in $Pr_5Ni_2Si_3$ ($n=3$) than in $Pr_{15}Ni_7Si_{10}$ ($n=4$), indicating a progression in the structure series.

In this paper, we report on the magnetic properties of solution-grown single-crystalline $Pr_6Ni_2Si_3$, the $n=2$ member of the aforementioned structure series. Results of specific heat and of extensive anisotropic magnetization measurements are presented. Moreover, measurements of the magnetization vector have been used to clarify the low-temperature magnetic order, which following crystallographic nomenclature[12] appears to be "exotic." Finally, the results are discussed within the systematics seen also for the $n=3$ and $n=4$ members of the series.

II. EXPERIMENT

Single crystals of $Pr_6Ni_2Si_3$ were grown out of a high-temperature ternary solution.[13–15] An initial alloy composition and a useful temperature range for growth were determined by means of combined differential thermal analysis and growth experiments.[16] The initial alloy composition used was $Pr_{60}Ni_{25}Si_{15}$, and the useful temperature range for growth was determined to be between ~1000 and ~880 °C. The starting elements were sealed in a three-cap Ta crucible,[15] which was sealed in an evacuated quartz ampoule. The ampoule was initially heated up to ~1200 °C to ensure a well-homogenized alloy, cooled to 1000 °C at ~50 °C/h, and then cooled down to 880 °C at 3 °C/h. The ampoule was taken out of the furnace, inverted, and centrifuged, resulting in a separation of crystals from an excess liquid. Crystals have a hexagonal-prismatic growth habit with faces parallel to the [001] crystallographic direction and normal to the [110] direction.[17] The crystals were up to 10 mm long and had effective diameters of up to 1 mm. A photograph of a $Pr_6Ni_2Si_3$ crystal is displayed in Fig. 1.

For initial characterization, we measured a powder x-ray diffraction pattern on finely ground crystals from the growth yield with a Rigaku Miniflex+diffractometer employing Cu $K\alpha$ radiation. The pattern was analyzed with RIETICA (Ref. 18) using a Le Bail-type[19] refinement, and it was indexed according to the space group $P63/m$, with lattice parameters $a=11.96(2)$ Å and $c=4.27(1)$ Å. These results are consistent with those reported earlier by Bodak *et al.*[20] who found $a=12.005$ Å and $c=4.273$ Å.

Specific heat was determined in a Quantum Design physical property measurement system at temperatures between 2 and 70 K. Magnetization measurements were performed using Quantum Design magnetic property measurement system magnetometers (QD-MPMS) in magnetic fields up to 5 T and at temperatures between 5 and 300 K. For most of the experiments described below, only the magnetization component parallel to the applied field was measured for samples aligned with the applied field parallel and perpendicular to the hexagonal *c* axis. To investigate a possible in-plane magnetic anisotropy, the sample was aligned with the field perpendicular to the *c* axis and rotated by means of a horizontal-axis rotator around the *c* axis.

Generally, a magnetization vector can be decomposed into three perpendicular vector components. We can distinguish a longitudinal component, along the applied field direction, here called M_L, and transverse components in the plane perpendicular to the applied field, here called M_X and M_Y. We used a QD-MPMS-5 system, which was equipped with both a conventional longitudinal pick-up-coil system and a transverse pick-up-coil system. Since the magnetometer is equipped with one single transverse pick-up-coil system, we used the vertical-axis sample rotator to determine both the M_X and the M_Y components of magnetization. For these vector measurements, the sample was aligned with the unique *c* axis at an angle of about 60° with the applied field direction.

III. RESULTS

Temperature-dependent specific heat is presented in Fig. 2(a). It will be shown below that $Pr_6Ni_2Si_3$ orders ferromagnetically. Then an onset criterion[21] for a peak in specific heat can be used. The peak in specific heat shows an onset temperature close to 40 K. A lattice contribution to specific heat, also shown, was estimated with the Debye model, and following Ref. 10, which gives a Debye temperature close to 200 K for both other members of the structure series of interest, we used a Debye temperature of $\Theta_D=209$ K. An electronic contribution was ignored. An estimate, Fig. 2(b), for the magnetic contribution per Pr ion C_M was obtained by subtracting this lattice contribution from the measured specific heat. Notice that, besides the peak near 40 K, also a shoulder with a maximum around 30 K can be observed. The temperature-dependent magnetic entropy S_M, estimated by integrating C_M/T up to 70 K and displayed in the inset of Fig. 2(b), gives a value of close to $R \ln 3$ at ~40 K and increases with increasing temperature, reaching a value of close to $R \ln 4$ at ~70 K. These results indicate that, aver-

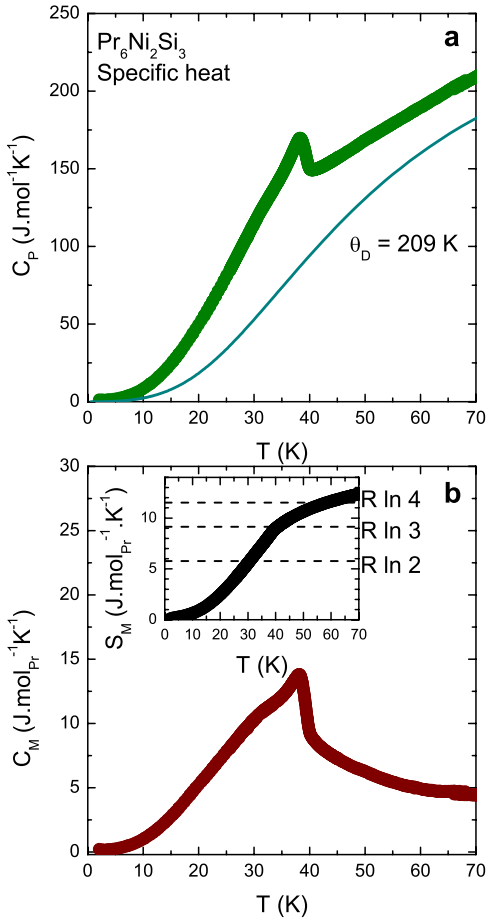

FIG. 2. (Color online) (a) Zero-field specific heat C_p as a function of temperature; also included is an estimate of the lattice specific heat. The mean-field-like with an onset near $T=40$ K is close to the Curie temperature. (b) Magnetic specific heat per Pr ion obtained from a. Note the shoulder between 30 and 35 K. The inset shows the estimated magnetic entropy to reach values close to R ln 3 at the ordering temperature.

aged over the two crystallographically distinct Pr ions, three states, likely a singlet and a doublet, are responsible for the magnetic order in this compound. Details of the crystal-field-induced $4f$ ground states of the distinct Pr ions will need to be determined in a separate experiment, e.g., by inelastic neutron scattering.

Figure 3 shows temperature-dependent magnetization measured upon cooling in a field of 0.01 T applied both parallel and perpendicular to the c axis. Two features are immediately obvious: the magnetization parallel to the c axis indicates a ferromagnetic component $\| c$ axis below ~40 K, and the magnetization $\perp c$ axis is much smaller than the magnetization parallel to the c axis, especially below 40 K, which indicates that the magnetic anisotropy in this compound is very large and favors the moments to align themselves parallel to the c axis.

Temperature-dependent magnetization for both these sample alignments was determined in various fields up to 5 T. From these it was found that above 50 K, the magnetization for both alignments increases linearly with increasing fields; thus, a differential magnetic susceptibility $\chi_{\text{diff}}=\frac{\Delta M}{\Delta H}$

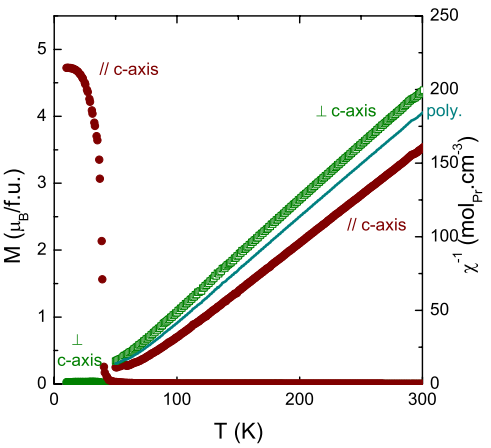

FIG. 3. (Color online) Closed circles, left axis: $Pr_6Ni_2Si_3$ temperature-dependent magnetization measured in 0.01 T, both for $H\|c$ axis (top) and for $H\perp c$ axis (bottom). Open circles, right axis: temperature-dependent inverse differential susceptibility determined for $H\|c$ axis (bottom) and $H\perp c$ axis (top) together with polycrystalline average χ^{-1} (center).

could be determined. A polycrystalline average was obtained by averaging $\chi\|c$ axis and $\chi\perp c$ axis according to $\chi_{\text{avg}}=(\chi_{\|}+2\chi_{\perp})/3$.

Figure 3 also shows the inverted temperature-dependent differential magnetic susceptibilities $\|$ c axis, $\perp$ c axis, and polycrystalline average. All three are linear, though not parallel, with temperature above 100 K, thus can be described by a Curie–Weiss law. The effective moments calculated for χ_{avg}, $\chi_{\|}$, and $\chi_{\perp}$ equal $3.35\mu_B$/Pr, $3.50\mu_B$/Pr, and $3.26\mu_B$/Pr, which are all not too far from the theoretical free-ion value for $(3.58\mu_B)$, thus indicating that the magnetism in $Pr_6Ni_2Si_3$ is determined by Pr local magnetic moments, and not significantly by Ni. However, the fact that the calculated effective moments are different for the different crystallographic directions is an indication of a substantial crystal-field splitting of the $2J+1$ levels of the Pr $4f$ shell, which is still noticeable at room temperature. Weiss temperatures Θ of 41, 53, and 33 K were found for Θ_{avg}, $\Theta_{\|}$, and $\Theta_{\perp}$, respectively, positive values which are reasonably close to T_C, and which indicate (mainly) ferromagnetic interactions between the Pr moments.

A. $H\|c$ axis

The Curie temperature for the onset of ferromagnetic order $\|$ c axis can be determined from Arrott plots.[22] Figure 4 shows such plots for $Pr_6Ni_2Si_3$, obtained from magnetization isotherms $H\|c$ axis in fields up to 500 Oe. According to Arrott's criterion,[22] precisely at T_C, the magnetic susceptibility χ tends to infinity, causing terms of M^3 to be dominant at low enough H. In other words, the Curie temperature is at that temperature where H-dependent M^3 is exactly linear starting at $H=0$. A criterion for the linearity of a fit line is given by the regression factor R, which ranges between 0 and 1, where 1 indicates a perfect line. Figure 4 shows M^3 vs H taken at temperatures between 39 and 41 K, and the inset shows the temperature-dependent R of such linear fits. From

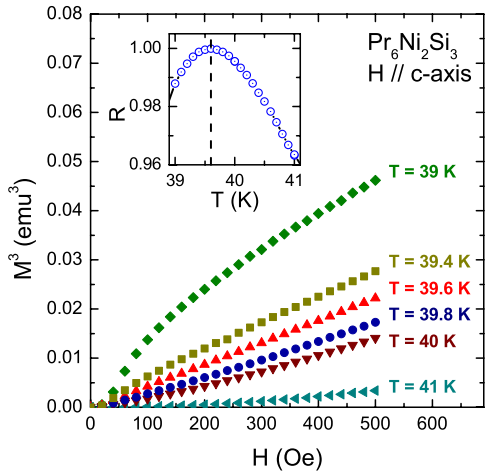

FIG. 4. (Color online) $Pr_6Ni_2Si_3$ Arrott plots for $H\|c$ axis, shown as field (H) dependent magnetization (M^3) for representative temperatures. The inset shows the T-dependent regression factor R for a linear fit through $M^3(T)$, indicating the Curie temperature $T_C=39.6(1)$ K.

this the Curie temperature is determined as $T_C=39.6(1)$ K. This value agrees very well with the above obtained value for the onset of the specific heat peak.

Hysteretic behavior of $Pr_6Ni_2Si_3$ at 1.8 K for $H\|c$ axis is shown in Fig. 5. These results were obtained by cooling the aligned crystal in zero field and measuring first the virgin magnetization curve. The observed presence of high coercivity in conjunction with the small slope of the virgin curve can be taken as a signature of the presence of narrow domain

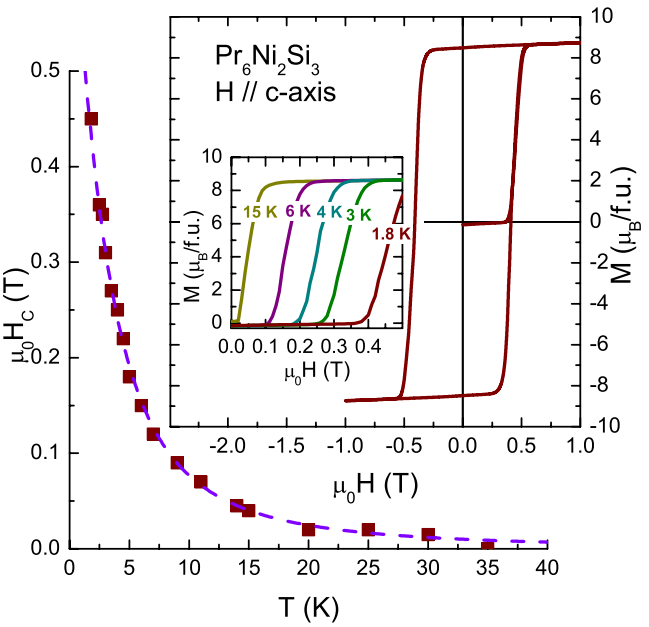

FIG. 5. (Color online) Top right: $Pr_6Ni_2Si_3$ zero-field-cooled magnetization loop for $H\|c$ axis at 1.8 K. The inset shows the development of virgin magnetization with temperature, demonstrating the coercive behavior. Bottom left: temperature-dependent coercive field for $H\|c$ axis. The line is obtained as described in the text.

walls.[23–27] Such narrow walls can be strongly pinned by magnetic obstacles of atomic dimensions. The strong increase in the magnetization on the virgin curve at $H_P=0.45$ T marks the propagation field H_P at which the external field is able to detach the narrow walls from the pinning sites. At higher fields the walls are removed from the crystal. Upon decreasing the fields from 1 T into the region of negative fields, reversed domains and domain walls can nucleate but the movement of these walls is impeded by the pinning sites so that the reversed domains cannot grow. This becomes possible again only for negative fields equal in magnitude to H_P, causing the absolute value of the coercive field to be equal to the propagation field, $H_C=H_P$.

Because of the strong hysteresis, the spontaneous magnetization M_S at 1.8 K can directly be obtained from this figure. It equals about $8.5\mu_B$/f.u., amounting to about $1.4\mu_B$/Pr ion, if the Pr ions on both Pr sites contribute, or, as will be discussed below, to about $2.8\mu_B$/Pr ion, if the Pr ions on one of the two sites are considered to contribute. These values are lower than the free-ion value of $3.2\mu_B$/Pr, which may be related to crystal-electric-field effects and the low point symmetry of both Pr-crystallographic sites. The temperature dependence of the coercive field is demonstrated in the inset of Fig. 5, which shows virgin $M(H)$ at different temperatures below 15 K. Note that besides having a different coercive field these curves overlap, so M_S is almost temperature independent below 15 K.

Measurements at various temperatures below T_C indicate the same behavior as at 1.8 K, but with a strongly temperature-dependent H_C Figure 5 shows temperature-dependent H_C. According to a model proposed by Barbara and Uehara,[26] the temperature dependence of coercivity can be described as

$$H_C^{-1}(T)=H_C(0)^{-1}+\alpha T, \tag{1}$$

where α is proportional to the spontaneous magnetization divided by the domain-wall energy, $\alpha\propto M_S/\gamma^2$. γ^2 in turn is proportional to the product of the average exchange energy and the average anisotropy energy. The inset of Fig. 5 shows temperature-dependent H_C^{-1} at temperatures between 1.8 and 15 K. A very good fit to this line is given by a second-order polynomial, and when comparing to Eq. (1), this means that α is linearly dependent on T. Values found are $H_C(0)^{-1}=1.4(3)$ T^{-1} and $\alpha(T)=0.37(9)+0.079(6)T$, leading to a zero-temperature H_C of 0.71 T. The dotted line in the main Fig. 5 was calculated using these values.

Since it is constant below 15 K, M_S is not expected to contribute to variations of $\alpha(T)$ below 15 K. Therefore, the variations in α below 15 K have to be proportional to the variations of $1/\gamma^2$, the inverted product of the average exchange energy, and the average anisotropy energy. Both the exchange energy and the anisotropy energy may be expected to decrease with increasing temperature, leading to α growing with increasing temperature.

B. $H\perp c$ axis

Figure 6 shows temperature-dependent magnetization for $H\perp c$ axis measured, with temperature decreasing, in various

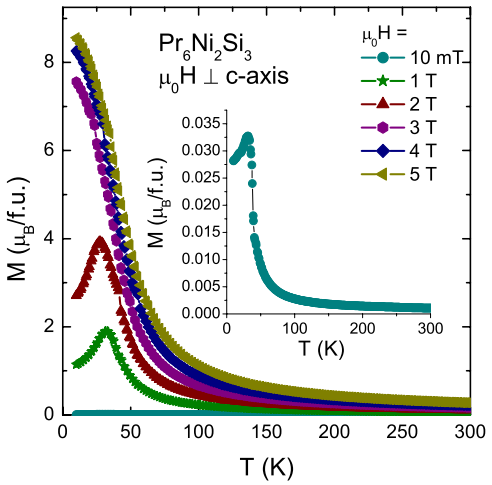

FIG. 6. (Color online) Temperature-dependent magnetization for $H \perp c$ axis measured in various fields up to 5 T. Note the maxima for 0.01 (≈32 K), 1 (≈32 K), and 2 T (≈27 K).

fields up to 5 T. In 0.01, 1 and 2 T, the magnetization shows a maximum, which appears close to 32 K for 0.01 and 1 T, and close to 27 K for 2 T. In 3 T and higher, no maximum is observed. Such behavior, a maximum in temperature-dependent magnetization, which shifts to lower temperature with increasing field strengths, is common in antiferromagnets.[28] Note also that the maximum in the 0.01 T curve occurs at a temperature close to the 32 K shoulder in specific heat.

Field-dependent magnetization isotherms for $H \perp c$ axis at temperatures between 5 and 45 K are shown in Fig. 7. At 5 K, starting in zero field, the magnetization starts at zero and first increases weakly and linearly with increasing field. Close to 2 T, the magnetization starts to increase much faster with increasing field, a process which ends close to 3 T, above which the magnetization continues to increase linearly with increasing field, at a slope similar to the slope in low

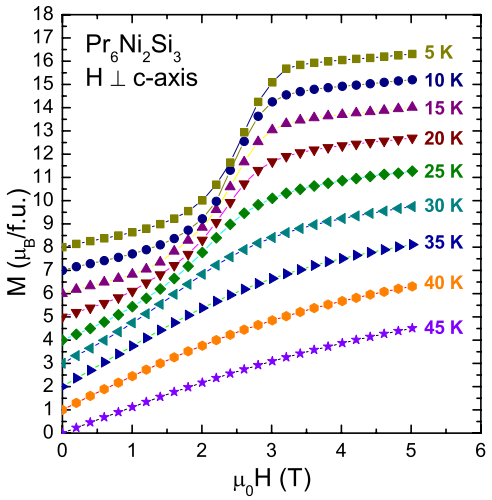

FIG. 7. (Color online) Field-dependent magnetization of $Pr_6Ni_2Si_3$ at various temperatures measured with $H \perp c$ axis. For clarity, the curves have been shifted by $1\mu_B$/f.u. with respect to one another.

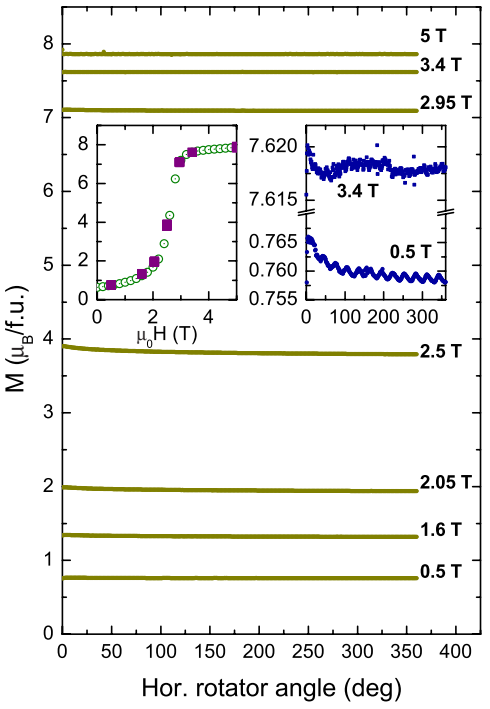

FIG. 8. (Color online) $Pr_6Ni_2Si_3$ horizontal-angle dependent magnetization, measured at 5 K, in various fields ($H \perp c$ axis) up to 5 T. The left inset shows all data as a function of H, superimposed on a denser data set measured at zero angle. The right inset shows a zoom in of the 0.5 T data (bottom) and the 3.4 T data (top).

field. As temperature increases, this process becomes less pronounced, resulting in a weakly s-shaped magnetization at 30 K, and a featureless magnetization at 35 K and higher. Also these results are consistent with the magnetization of a simple antiferromagnet, and the magnetization process could be interpreted as due to a spin flop.[28]

To determine magnetic anisotropy in the plane perpendicular to the c axis, we more precisely measured the magnetization at 5 K for the field $\perp$ c axis with a horizontal rotator, rotating the sample around the c axis. In a hexagonal system with a very strong in-plane anisotropy, the in-plane magnetization may vary by as much as $1-\cos 30° \sim 15\%$. Figure 8 shows the magnetization in various fields up to 5 T, measured at horizontal rotator angles between 0° and 360°. For all chosen field strengths, the variation in magnetization is smaller that the symbols used for the figure. The in-plane anisotropy of $Pr_6Ni_2Si_3$ in fields up to 5 T is thus very small, which is exemplified in the left inset, by plotting all thus measured magnetization values on a more densely measured field-dependent magnetization curve, measured at zero angle. Strongly zoomed in, see right inset of Fig. 8, e.g., the magnetization at 0.5 T shows a very weak and 12-fold variation, with an amplitude of variation of about 0.1%. This variation disappears in higher fields: the zoomed in angular dependent magnetization measured in 3.4 T shows no such variation. This 12-fold variation may be related to the two crystallographically distinct magnetic Pr sites in the unit cell of $Pr_6Ni_2Si_3$.

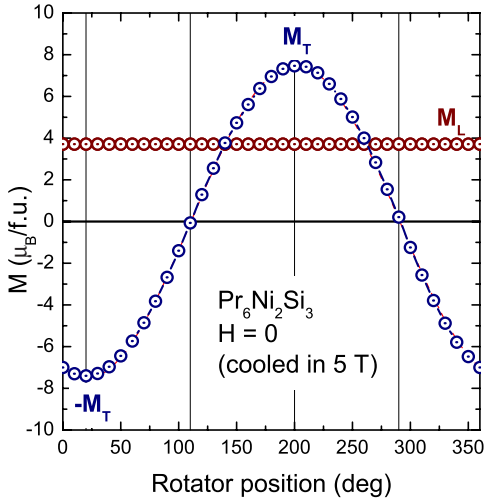

FIG. 9. (Color online) $Pr_6Ni_2Si_3$ zero-field magnetization, measured at 5 K both parallel to the applied field H (M_L) and perpendicular to it (M_T) as a function of (vertical) rotator position. This was measured on a field-cooled sample which was mounted with its c axis at an angle of approximately 60° with H.

C. H applied at 60° from the c axis

The crystal was mounted and centered in a straw such that the applied field H made an angle of ≈60° with the c-axis. The very weak in-plane anisotropy, Fig. 8, made it clear that no particular attention to the planar direction closest to the applied field was necessary, which is not true if the in-plane anisotropy is strong.[29] The sample was then cooled in an applied field of 5 T from room temperature to 5 K, at which temperature the field was removed. Vertical-rotator angle-dependent zero-field magnetization measured both parallel (longitudinal magnetization M_L) and perpendicular to H (transverse magnetization M_T) are shown in Fig. 9. Whereas the measured M_L is vertical-angle independent, M_T is determined as the amplitude of the measured transverse magnetization cosine. We thus find for M_T a value of $\approx 7.5\mu_B$/f.u. and for M_L $3.8\mu_B$/f.u. The angle of the magnetic moment with the applied field is given by $\tan^{-1}\frac{M_T}{M_L}=63°$, which is in good agreement with the angle at which the crystal axis was mounted in the sample holder. The size of the moment vector $|M|=\sqrt{M_L^2+M_T^2}=8.4\mu_B$/f.u. is in excellent agreement with the magnetization moment found at 5 K for $H\|c$ axis.

Field-dependent magnetization was determined by measuring both M_L and M_T at 5 K in various H up to 5 T. M_L was determined in the conventional way. Full rotations of the vertical rotator, similar to the measurement shown in Fig. 9, were made to determine M_T. In this way, we verified that the magnetic moment does not rotate in the plane perpendicular to the magnetic field, which was a distinct possibility.[29] The results are shown in Fig. 10. As expected, M_L increases uniformly with increasing H, and the spin-flop-like transition starts close to 2.5 T, a field some 15% (=1/sin 60°) higher than for the measurement shown in Fig. 7. At the same time, M_T decreases uniformly with increasing fields, which generally indicates a rotation of the magnetic moment toward H. The spin-flop-like transition for this magnetization-vector component mimics the one for M_L, but as a stronger decrease rather than an increase. The amount by which the magnetization vector decreases for M_T due to the spin-flop-like transition may seem small compared to the increase observed for M_L. This is clarified examining the total magnetization, the vector sum $|M|$, also shown in Fig. 10. $|M|$ shows a small, linear increase with increasing field strengths up to ~2.5 T, and increases even further during the spin-flop-like transition, up to about 3.5 T, above which it further increases slightly and linearly. This anomalous change in length of the magnetization vector is an immediate indication that the metamagnetic spin-flop-like transition for $H\perp c$ axis is not due to a simple rotation of the magnetization vector.[29]

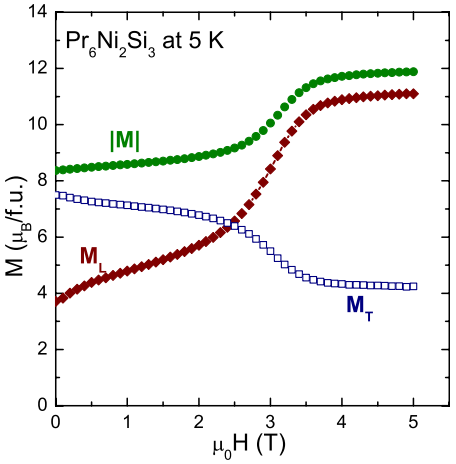

FIG. 10. (Color online) $Pr_6Ni_2Si_3$ field-dependent magnetization, measured at 5 K both parallel (M_L) and perpendicular (M_T) to the applied field, resulting in a vector-summed magnetization $|M|$.

Figure 11 shows the measured field-dependent magnetization vector with the field applied at ~60° from c axis (Fig. 10) decomposed[29] in a component ∥ c axis and a component

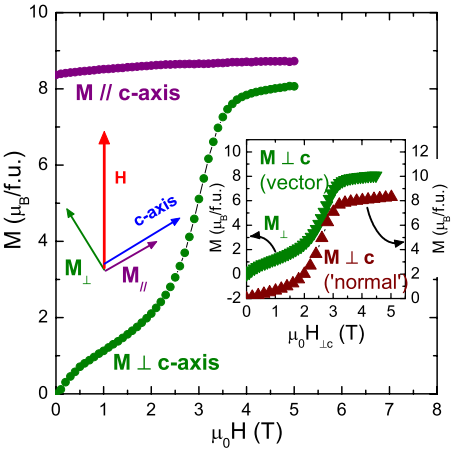

FIG. 11. (Color online) $Pr_6Ni_2Si_3$ field-dependent magnetization, both parallel and perpendicular to the c axis, determined from Fig. 10. The inset shows the magnetization ⊥ c axis as a function of the field-component ⊥ c axis, compared to magnetization ⊥ c axis measured with the field applied ⊥ c axis.

$\perp c$ axis. For comparison, field-dependent longitudinal magnetization measured with H applied $\| c$ axis and with H applied $\perp c$ axis are shown in the inset of Fig. 11. We show an almost constant magnetization $\| c$ axis, whereas the magnetization $\perp$ shows a spin-flop-like transition. The inset of the lower panel of Fig. 11 shows the magnetization $\perp c$ axis obtained by vector magnetometry with H projected $\perp c$ axis, compared to the longitudinal magnetization from the upper panel of Fig. 11. Thus, the spin-flop-like process $\perp c$ axis occurs independent from the magnetization $\| c$ axis and is only due to $H \perp c$ axis. Note that the value of $M \perp c$ axis above 4 T is close to $8\mu_B$/f.u., which is close to the saturation magnetization $\| c$ axis, which amounts, as above, to about $1.3\mu_B$/Pr if Pr ions on both Pr sites contribute or $2.7\mu_B$/Pr if Pr ions on only one of the two sites contribute.

IV. DISCUSSION AND CONCLUSIONS

The experimental results shown above indicate quite clearly that the magnetic order in the intermetallic compound $Pr_6Ni_2Si_3$ has both ferromagnetic and antiferromagnetic components, which may be called "exotic" following proposed nomenclature.[12] We propose that the ferromagnetic order involves one of the two Pr sites, and the antiferromagnetic order the other one, which we will discuss in more detail below. If this is the case, the ordered moment for both sites is close to $2.7-2.8\mu_B$/Pr, which is not too far from the theoretical $g_J J$ value for Pr: $3.2\mu_B$.

Two magnetic phase transitions may be discerned. The first transition occurs at T_C=39.6 K, where Pr moments order ferromagnetically $\| c$ axis. This transition is evidenced by a clear specific-heat anomaly and by the Arrott plots of $M(H)$ for $H \| c$ axis. The second magnetic transition is due to antiferromagnetic order $\perp c$ axis and shows as a weak shoulder in specific heat close to 32 K, and in low fields $\perp c$ axis by $M(T)$, where a peak occurs close to 32 K. Furthermore, spin-flop-like transitions are only clearly observed below 32 K.

The ferromagnetic order $\| c$ axis is further corroborated by the strong and strongly temperature-dependent coercivity that occurs for $M \| c$ axis, which shows itself in nearly square magnetization loops at low temperatures. Such loops occur in anisotropic ferromagnets with narrow domain walls which are strongly pinned on obstacles of atomic size. The coercivity in $Pr_6Ni_2Si_3$ becomes stronger with decreasing temperatures, which may be expected for any coercive magnet. We find no clear evidence that the behavior of the coercive field is related to the development of antiferromagnetic order $\perp c$ axis. The cause of the narrow domain walls, which are not usually observed in pure single crystals, is not presently clear but may be related to the intrinsic crystallographic disorder we have found.[6,17] The magnetic anisotropy for the ordered component $\| c$ axis is very large at low temperatures, which is corroborated by the measurements of the magnetization vector for H applied at an angle of 60° with the c axis, which indicated that the magnetization component $\| c$ axis was almost unaffected by fields equivalent to over 4 T $\perp c$ axis.

The antiferromagnetic order $\perp c$ axis in turn is corroborated by a magnetization process, similar to a spin-flop transition, which starts close to 2 T at 2 K for $H \perp c$ axis. That this magnetization process is only due to magnetization for $H \perp c$ axis is evidenced by measurements of the magnetization vector for H applied at an angle of 60° with the c axis. Also this antiferromagnetically ordered-moment component is highly anisotropic because the low-temperature magnetization measured with $H \| c$ axis is almost field independent in fields up to 1 T (see Fig. 5).

The magnetic properties of single-crystalline $Pr_6Ni_2Si_3$ are consistent with the (polycrystalline) magnetic properties of the other members of the structure series, $Pr_5Ni_2Si_3$ and $Pr_{15}Ni_7Si_{10}$, which order also ferromagnetically at 50 and 60 K, respectively (see Refs. 7 and 8). Both compounds show a pronounced coercivity which develops as temperature decreases. Both these compounds also show, besides the Curie-temperature anomaly, shoulders in specific heat, at 27 and at 33 K, respectively, below which temperatures for both these compounds in the magnetization metamagneticlike behavior appears. As $Pr_5Ni_2Si_3$ and $Pr_{15}Ni_7Si_{10}$ are members of the same structure series as $Pr_6Ni_2Si_3$, these results can be interpreted as follows: the ferromagnetic component in both compounds is parallel to the c axis. The coercive behavior of both compounds is associated with the ferromagnetic component $\| c$ axis and may be due to the same mechanism as the one in $Pr_6Ni_2Si_3$. The shoulder in specific heat, occurring for both $Pr_5Ni_2Si_3$ and $Pr_{15}Ni_7Si_{10}$, then is due an antiferromagnetic order perpendicular to the c axis, which then is responsible for the metamagneticlike behavior.

As mentioned in Sec. I, this metamagneticlike behavior is more pronounced in $Pr_5Ni_2Si_3$ than in $Pr_{15}Ni_7Si_{10}$. This can be understood as follows: there is one Pr-site type that occurs exactly one time in all three members of the structure series, the site that is comparable to Pr1 or "corner"[9] in Fig. 1. We therefore propose that in all three members of the structure series, $Pr_6Ni_2Si_3$, $Pr_5Ni_2Si_3$, and $Pr_{15}Ni_7Si_{10}$, the ferromagnetic order $\| c$ axis is determined by the "noncorner" Pr sites, and the antiferromagnetic order $\perp c$ axis is determined by the corner sites in these compounds. Note that although our results are somewhat different than the calculated model structures proposed recently Jiles and Song,[9] they also noted that the corner site may be involved in antiferromagnetic order $\perp c$ axis.

In conclusion, the above presented results on $Pr_6Ni_2Si_3$ indicate that its ordered state manifests both ferromagnetic and antiferromagnetic components. The results are not only consistent with results obtained on other members of the structure series of which it forms part but also clarifies these.

ACKNOWLEDGMENTS

We are indebted to S. L. Bud'ko, Y. Mozharivskyj, and J. Frederick for valuable discussions and for help with the experiments. Ames Laboratory is operated for the U.S. Department of Energy by Iowa State University under Contract No. W-7405-Eng-82. This work was supported by the Director for Energy Research, Office of Basic Energy Sciences.

*yjanssen@bnl.gov. Present address: Brookhaven National Laboratory, Upton, New York 11973, USA.

[1] P. G. de Gennes, J. Phys. Radium **23**, 510 (1962).
[2] J. Jensen and A. R. Mackintosh, *Rare Earth Magnetism* (Clarendon, Oxford, 1991).
[3] K. N. R. Taylor, Adv. Phys. **20**, 551 (1971).
[4] E. Parthé and B. Chabot, in *Handbook on the Physics and Chemistry of Rare Earths*, edited by K. A. Gschneidner, Jr. and L. Eyring (North-Holland, Amsterdam, 1984), Vol. 6, p. 113.
[5] T. C. Ozawa and S. J. Kang, J. Appl. Crystallogr. **37**, 679 (2004).
[6] D. Wu, M. Huang, T. A. Lograsso, R. W. McCallum, Y. Mozharivski, and A. Llobet, J. Alloys Compd. **441**, 206 (2007).
[7] A. O. Pecharsky, Y. Mozharivskyj, K. W. Dennis, K. A. Gschneidner, R. W. McCallum, G. J. Miller, and V. K. Pecharsky, Phys. Rev. B **68**, 134452 (2003).
[8] D. C. Jiles, S. H. Song, J. E. Snyder, V. K. Pecharsky, T. A. Lograsso, D. Wu, A. O. Pecharsky, Y. Mudryk, K. W. Dennis, and R. W. McCallum, J. Magn. Magn. Mater. **299**, 288 (2006).
[9] D. C. Jiles and S. H. Song, J. Appl. Phys. **101**, 023918 (2007).
[10] S. H. Song, D. C. Jiles, J. E. Snyder, A. O. Pecharsky, D. Wu, K. W. Dennis, T. A. Lograsso, and R. W. McCallum, J. Appl. Phys. **97**, 10M516 (2005).
[11] S. H. Song, J. E. Snyder, D. Wu, T. A. Lograsso, K. W. Dennis, R. W. McCallum, Y. Janssen, and D. C. Jiles, IEEE Trans. Magn. **41**, 3499 (2005).
[12] J. C. Tolédano, R. S. Berry, P. J. Brown, A. M. Glazer, R. Metselaar, D. Pandey, J. M. Perez-Mato, R. S. Roth, and S. C. Abrahams, Acta Crystallogr., Sect. A: Found. Crystallogr. **57**, 614 (2001).
[13] Z. Fisk and J. P. Remeika, in *Handbook on the Physics and Chemistry of Rare Earths*, edited by K. A. Gschneidner, Jr. and L. Eyring (North-Holland, Amsterdam, 1989), Vol. 12.
[14] P. C. Canfield and Z. Fisk, Philos. Mag. B **65**, 1117 (1992).
[15] P. C. Canfield and I. R. Fisher, J. Cryst. Growth **225**, 155 (2001).
[16] Y. Janssen, M. Angst, K. W. Dennis, R. W. McCallum, and P. C. Canfield, J. Cryst. Growth **285**, 670 (2005).
[17] Y. Mozharivskyj (unpublished).
[18] B. Hunter, LHPM-RIETICA (www.rietica.org).
[19] A. Le Bail, H. Duroy, and J. L. Fourquet, Mater. Res. Bull. **23**, 447 (1988).
[20] O. I. Bodak, E. I. Gladyshevskii, and O. I. Kharchenko, Sov. Phys. Crystallogr. **19**, 45 (1974).
[21] E. Morosan, S. L. Budko, and P. C. Canfield, Phys. Rev. B **72**, 014425 (2005).
[22] A. Arrott, Phys. Rev. **108**, 1394 (1957).
[23] B. Barbara, C. Bécle, R. Lemaire, and D. Paccard, J. Phys. C **1**, 299 (1971).
[24] T. Egami and C. D. Graham, J. Appl. Phys. **42**, 1299 (1971).
[25] J. J. van den Broek and H. Zijlstra, IEEE Trans. Magn. **7**, 226 (1971).
[26] B. Barbara and M. Uehara, IEEE Trans. Magn. **12**, 997 (1976).
[27] O. Tegus, Y. Janssen, E. Bruck, A. A. Menovsky, F. R. de Boer, and K. H. J. Buschow, J. Alloys Compd. **317-318**, 459 (2001).
[28] L. J. de Jongh and A. R. Miedema, Adv. Phys. **23**, 1 (1974).
[29] Y. Janssen, J. C. P. Klaasse, E. Brück, F. R. de Boer, K. H. J. Buschow, J. Kamarád, and N. V. Kudrevatykh, Physica B (Amsterdam) **319**, 59 (2002).